# Multi-Frequency Millimeter Wave Massive MIMO Channel Measurements and Analysis

Jie Huang[1], Rui Feng[1], Jian Sun[1,2], Cheng-Xiang Wang[1,3], Wensheng Zhang[1], and Yang Yang[4]
[1]Shandong Provincial Key Lab of Wireless Communication Technologies, Shandong University, Jinan, 250100, China.
[2]State Key Lab. of Millimeter Waves, Southeast University, Nanjing, 210096, China.
[3]Institute of Sensors, Signals and Systems, School of Engineering & Physical Sciences, Heriot-Watt University, Edinburgh, EH14 4AS, UK.
[4]Shanghai Research Center for Wireless Communications (WiCO), Shanghai, 201210, China.
Email: hj_1204@sina.cn, fengxiurui604@163.com, sunjian@sdu.edu.cn, cheng-xiang.wang@hw.ac.uk, zhangwsh@sdu.edu.cn, yang.yang@wico.sh

***Abstract*—Massive multiple-input multiple-output (MIMO) technology and millimeter wave (mmWave) communication are key technologies for the fifth generation (5G) wireless communications. The combination of mmWave and massive MIMO has the potential to dramatically improve wireless access and throughput performance. Such systems benefit from large available signal bandwidths and small antenna form factor. In the literature, most of the massive MIMO channel measurements are carried out at sub-6 GHz frequency bands, while the effects caused by large antenna arrays at mmWave bands have not been studied yet. In this paper, we conduct channel measurements at 11, 16, 28, and 38 GHz frequency bands combined with large antenna arrays in an indoor office environment. The space-alternating generalized expectation-maximization (SAGE) algorithm is applied to obtain the multipath component (MPC) parameters. New propagation characteristics like spherical wavefront, cluster birth-death, and non-stationarity over antenna array axis are validated for the four mmWave bands by investigating the temporal-spatial channel characteristics like power delay profile (PDP), power azimuth profile (PAP), power elevation profile (PEP), root mean square (RMS) delay spread (DS), and azimuth and elevation angular spread (AS). The results indicate that massive MIMO effects should be fully considered for mmWave channel models under systems with large antenna arrays.**

***Index Terms*—Millimeter wave, massive MIMO, channel measurements, non-stationarity, SAGE.**

## I. Introduction

Massive MIMO technology and mmWave communication are key technologies for the 5G wireless communications [1]. MmWave generally corresponds to 30–300 GHz frequency bands, but sometimes 10–30 GHz frequency bands are also included as they share some similar propagation characteristics [2]. Massive MIMO technology has the potential to enable substantial improvements in spectral and energy efficiency. In a typical massive MIMO system, single-antenna mobile stations (MSs) communicate with a base station (BS) equipped with a large number of antennas [3]. By exploiting the spatial degrees of freedom arising from the massive BS antennas, MSs can be served simultaneously and independently by using simple linear processing schemes.

The combination of mmWave and massive MIMO has the potential to dramatically improve wireless access and throughput performance [4]. Such systems benefit from large available signal bandwidths and small antenna form factor.

The radiation field of antennas is usually divided into the near field region (Fresnel zone) and far field region (Fraunhofer zone), which are defined by the Rayleigh distance. When the number of antennas at a BS increases to hundreds, the aperture of the antenna array becomes much larger, as compared to conventional MIMO systems with limited numbers of antennas. MSs and significant scatterers can locate within the Rayleigh distance of the large antenna array, and spherical wavefront rather than plane wavefront is experienced over the array. This is caused by the near field effect. The MPCs will have delay and angle drifts over the array. Moreover, clusters may appear and disappear over the array. Different antennas at the BS observe different sets of clusters in different time instants, which can be described by a birth-death process. The received powers of MPCs will vary over the array and show a non-stationarity property [5].

In order to verify these new propagation characteristics caused by large antenna arrays, experimental channel measurements have been carried out in the literature. In [6], outdoor channel measurements were conducted at 2.6 GHz by using a vector network analyzer (VNA) and a 128-element virtual uniform linear array (ULA). It showed that the received power varied over the array significantly, and the near field effects and non-stationarity over the array helped to decorrelate the channels for different users. In [7], outdoor channel measurements were conducted at 2.6 GHz for a 128-element real cylindrical patch antenna array with a RUSK channel sounder and for a 128-element virtual ULA with a VNA. The dirty-paper coding (DPC) capacities and zero-forcing (ZF) sum-rates were compared for these two antenna array configurations. In [8], outdoor channel measurements were conducted at 3.33 GHz by using a signal generator, a spectrum analyzer, and a 64-element virtual ULA. The non-stationarity of the channel over the array was identified both in delay and spatial domains. In [9], indoor channel measurements were conducted at 2, 4, and 6 GHz bands by using a signal generator, a spectrum analyzer, and a 64-element virtual ULA. The non-stationarity of the channel over the array was analyzed in the form of the variations of DS and coherence bandwidth. The impact of carrier frequency on channel parameters was also discussed.

However, all the above mentioned measurements were conducted at sub-6 GHz frequency bands with limited bandwidths, and new propagation characteristics caused by large antenna arrays have not been fully verified for mmWave bands. Recently, a 48-element active phased array antenna was used to measure the massive MIMO channel at 44 GHz [10]. The MPC parameters and transmit performance results using a cluster model were derived and analyzed. In [11], indoor channel measurements were conducted at 13–17 GHz bands by using a VNA and a $20 \times 20$-element virtual uniform rectangular array (URA). The variations of channel characteristics such as narrowband channel gain, K-factor, and DS across the array were investigated.

978-1-4673-8999-0/17/$31.00 ©2017 IEEE

These measurements are not sufficient to fully characterize the mmWave massive MIMO channels, and more comprehensive massive MIMO channel measurements should be conducted at mmWave bands. In this paper, we carry out massive MIMO channel measurements at 11, 16, 28, and 38 GHz bands in an indoor office environment. For each frequency band, the large antenna array is divided into several sub-arrays and processed with the SAGE algorithm. The key contributions of the paper are that the spherical wavefront, cluster birth-death, and non-stationarity properties over antenna array axis are investigated and validated for the four mmWave frequency bands.

The remainder of this paper is organized as follows. Section II describes the measurement environment and measurement system setup. In Section III, the SAGE algorithm and array data processing method are presented. The massive MIMO properties validation and analysis are described in Section IV. Finally, conclusions are drawn in Section V.

## II. MmWave Massive MIMO Channel Measurements

### A. Measurement Environment

The channel measurements are conducted in an indoor office environment with room size of $7.2\times7.2\times3$ $\mathrm{m}^3$, as shown in Fig. 1(a) [12]. The office is furnished with multiple chairs, desks, and a table. The desks are about 0.75 m high at desktop level but with an additional vertical clapboard having about 0.45 m height. Thus, the total height is about 1.2 m. In addition, the desks and table are equipped with several computers and electronic devices. Other large objects include a closet, an air conditioner, a water machine, and a whiteboard. The layout and sizes of main objects in the office are shown in Fig. 1(b). The walls, floor and ceiling are made of concrete. Parts of the floor and ceiling are made of anti-static-electricity board. There are several windows on both sides of the wall.

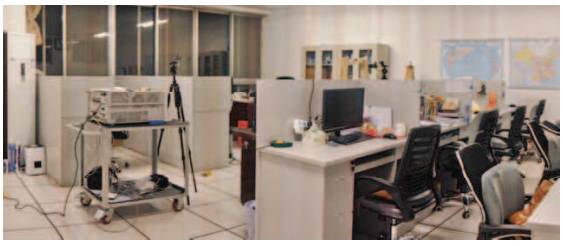

(a)

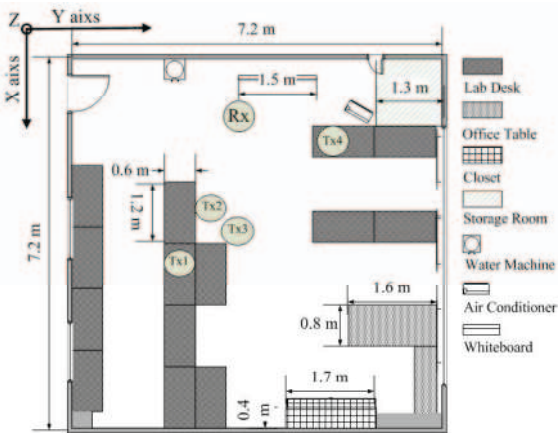


(b)

Fig. 1. (a) Photo of the environment and (b) layout of the environment.

### B. Measurement System Setup

The channel sounder consists of a Keysight N5227A VNA, a series of standard gain horn antennas, a biconical antenna, an antenna positioner, cables, connectors, a tripod, and a laptop. The VNA can sweep over a large frequency bandwidth within a short time. The intermediate frequency (IF) filter bandwidth is set to 500 Hz to reduce the power level of the noise floor. Port 1 of the VNA is connected to the transmitter (Tx) antenna by a cable and it sends the transmitted frequency sweeping signal, while Port 2 is connected to the receiver (Rx) antenna by a cable and it receives the fading signal. Thus, the $S_{21}$ parameter is the channel transfer function and the channel impulse response can be obtained by the inverse Fourier transform. The antenna locations are shown in Fig. 1(b). The coordinate of the Rx antenna is (1, 3, 1.45), and the coordinates of Tx antennas are (4, 2.2, 2.6), (3.2, 2.4, 2.6), (3.6, 3, 2.6), and (2, 5.2, 2.6), respectively. As a single horn antenna cannot cover the whole 10–40 GHz frequency bands, at the Tx side, four standard gain vertical polarized horn antennas working at 10–15, 15–22, 22–33, and 33–50 GHz bands are used to measure 11, 16, 28, and 38 GHz frequency bands, respectively. The antenna gain is 10 dB with a half power beamwidth (HPBW) of 55° to cover a large space. The Rx antenna is a vertical polarized biconical antenna working at 3–40 GHz bands with gain of 3 dB. Its radiation pattern is omni-directional for the whole bands. During the measurement, the Tx antenna is fixed and aligned to the center of the Rx large antenna array and placed on a tripod at four locations, while the Rx antenna is placed on an antenna positioner to shift positions to form a large virtual URA. The measurements are conducted automatically with the environment being kept quasi-static. Before the measurement, a back-to-back calibration is conducted by connecting the cables directly to remove the responses of the measurement system and the cables for each frequency band.

The measurement system setup for the four bands is shown in Table I, while the antenna array configuration is shown in Table II. For 11 and 16 GHz lower bands, the signal bandwidth is 2 GHz, the delay resolution is 0.5 ns, and the array size is $60\times60$ $\mathrm{cm}^2$. For 28 and 38 GHz higher bands, the signal bandwidth is 4 GHz, the delay resolution is 0.25 ns, and the array size is $36\times36$ $\mathrm{cm}^2$. The frequency resolution for the four bands is 5 MHz. The spacing steps for the four bands are 12, 8, 4, and 3 mm, which are within half-wavelength and about 0.44, 0.43, 0.37, and 0.38, respectively, when normalized to the corresponding wavelengths. The large URA is divided into several sub-arrays, and a sliding window is used over the array on Y axis. For the four bands, the calculated sub-array Rayleigh distances are within the Tx–Rx distances, which fulfil the far field and plane wavefront assumptions.

## III. Measurement Data Processing Methods

The maximum likelihood (ML) based SAGE algorithm [13] is applied to process the measurement data. The SAGE algorithm is valid based on plane wavefront assumption, i.e., when the Tx–Rx distance is beyond the Rayleigh distance and far field assumption is held. In this paper, we use the SAGE algorithm to

process sub-array measurement data when the Tx–Rx distance is beyond the Rayleigh distance. The sub-array was chosen to slide over the whole large array on Y axis. In the SAGE algorithm, the number of MPCs $L$ is usually predefined large enough to capture all the significant paths. A number of 100 MPCs was found to have a good trade-off between accuracy and computational complexity. The outputs of the SAGE algorithm are the parameter sets $\mathbf{\Theta}_l = [\alpha_l, \tau_l, \phi_l, \theta_l], l = 1, ..., L$, where $\alpha_l$, $\tau_l$, $\phi_l$, and $\theta_l$ denote the complex amplitude, delay, azimuth angle, and elevation angle for the $l$th MPC, respectively. These spatial-temporal MPC parameters are used to obtain some important propagation channel characteristics.

The PDP, PAP, and PEP can be obtained as

$$PDP = \sum_{l=1}^{L} |\alpha_l|^2 \, \delta(\tau - \tau_l) \tag{1}$$

$$PAP = \sum_{l=1}^{L} |\alpha_l|^2 \, \delta(\phi - \phi_l) \tag{2}$$

$$PEP = \sum_{l=1}^{L} |\alpha_l|^2 \, \delta(\theta - \theta_l) \tag{3}$$

where $\delta()$ is the Dirac delta function.

Note that the power of estimated MPCs with the same delay, azimuth angle, or elevation angle are summed up to get unique values.

The RMS DS is calculated as

$$DS = \sqrt{\frac{\sum_1^L |\alpha_l|^2 \tau_l^2}{\sum_1^L |\alpha_l|^2} - (\frac{\sum_1^L |\alpha_l|^2 \tau_l}{\sum_1^L |\alpha_l|^2})^2}. \tag{4}$$

Similarly, the RMS AS is calculated as

$$AS = \sqrt{\frac{\sum_1^L |\alpha_l|^2 \psi_l^2}{\sum_1^L |\alpha_l|^2} - (\frac{\sum_1^L |\alpha_l|^2 \psi_l}{\sum_1^L |\alpha_l|^2})^2} \tag{5}$$

where $\psi_l$ denotes the azimuth angle $\phi_l$ or elevation angle $\theta_l$.

TABLE I
MEASUREMENT SYSTEM SETUP.

| Center frequency (GHz) | 11 | 16 | 28 | 38 |
|---|---|---|---|---|
| Wavelength (mm) | 27 | 19 | 11 | 8 |
| Bandwidth (GHz) | 2 | 2 | 4 | 4 |
| Delay resolution (ns) | 0.5 | 0.5 | 0.25 | 0.25 |
| Output power (dBm) | 15 | 15 | 13 | 8 |
| Sweeping points | 401 | 401 | 801 | 801 |

TABLE II
ANTENNA ARRAY CONFIGURATION.

| Center frequency (GHz) | 11 | 16 | 28 | 38 |
|---|---|---|---|---|
| Spacing step (mm) | 12 | 8 | 4 | 3 |
| Array size ($cm^2$) | 60×60 | 60×60 | 36×36 | 36×36 |
| Array elements | 51×51 | 76×76 | 91×91 | 121×121 |
| Sub-array elements | 10×10 | 15×15 | 15×15 | 20×20 |
| Sliding window | 1:2:41 | 1:3:61 | 1:3:76 | 1:2:101 |
| Rayleigh distance (m) | 1.7 | 2.7 | 1.2 | 1.6 |

## IV. RESULTS AND ANALYSIS

For each frequency band, the SAGE algorithm is applied to process the sub-array data with a sliding window over the array on Y axis to find the new massive MIMO propagation characteristics. Especially, the spherical wavefront, cluster birth-death, and non-stationarity properties will be investigated and validated.

### A. Spherical Wavefront Property

Under far field or plane wavefront assumption, the electromagnetic waves propagate parallel to each other, thus the arrival angles of MPCs will be the same for all antenna elements. As the number of antennas increases to hundreds, the aperture of the antenna array becomes much larger. The Tx–Rx may be within the Rayleigh distance, and the far field or plane wavefront may be violated. Fig. 2 shows the line of sight (LOS) path azimuth angle variations for the four bands over the array on Y axis at the four Tx locations. For each Tx location, the angle drifts of the four bands show similar trends, and the rates of azimuth angle drift are about 23, 29, 27, and 10 $^\circ/m$ for the four Tx locations, respectively. These angle drifts can be verified by using simple triangular geometry relationships given the Tx and Rx settings. The LOS path elevation angle variations for the four bands at Tx4 is shown in Fig. 3. As the Tx–Rx distances are on the order of 3 m with the same antenna height differences for the four Tx locations, the LOS path elevation angle variations at the other 3 Tx locations show similar characteristics. The step-wise change of the angle is due to the fact that the azimuth and elevation angle resolution of the SAGE algorithm is set as $1^\circ$. An angle drift of as large as $10^\circ$ is observed for the azimuth and elevation angles, which indicates that the plane wavefront assumption is not valid and the spherical wavefront should be considered.

### B. Cluster Birth-Death Property

Certain clusters are not observable over the whole array, and each antenna element on the large array have its own set of clusters. The clusters may appear and disappear over the array axis, which can be described by a Markov birth-death process. Fig. 4, Fig. 5, and Fig. 6 show the cluster birth-death property of the PDP, PAP, and PEP variations over the array axis for 16 GHz band at Tx1 location, respectively. The LOS path and some first-order reflection MPCs can be seen over the array, while some MPCs are not observable at each antenna position. The results verify the cluster birth-death property for mmWave bands. As the measurement environment is kept quasi-static, the reason for cluster birth-death may be that as the antenna moves in a large area, the antenna cannot see all the objects in the environment. Thus, some small objects may be observed by the antenna at one position, while these objects may be out of the visible range of the antenna at another position. A more complex environment is more likely to observe the cluster birth-death property.

### C. Non-Stationarity Property

For massive MIMO systems, the wide sense stationary (WSS) assumption may be violated, and MPC parameters may vary over the large physical array. The variations of the LOS path received power over the array at Tx2 location is shown in Fig. 7. The LOS path received power can vary several dB

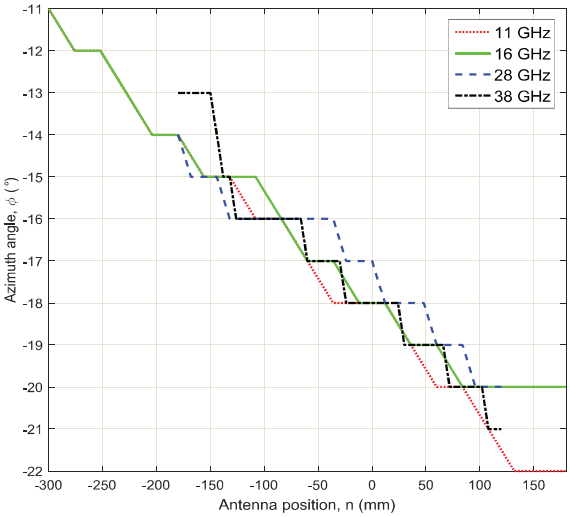


(a) Azimuth angle variations at Tx1

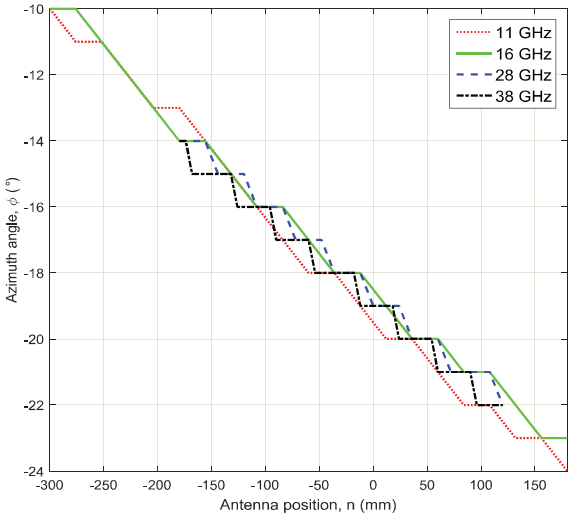


(b) Azimuth angle variations at Tx2

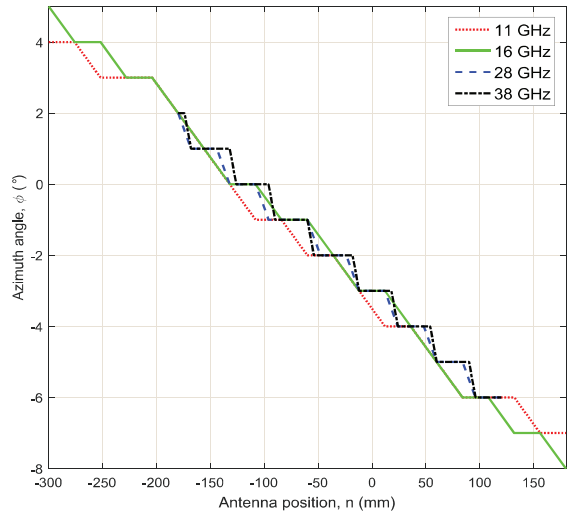


(c) Azimuth angle variations at Tx3

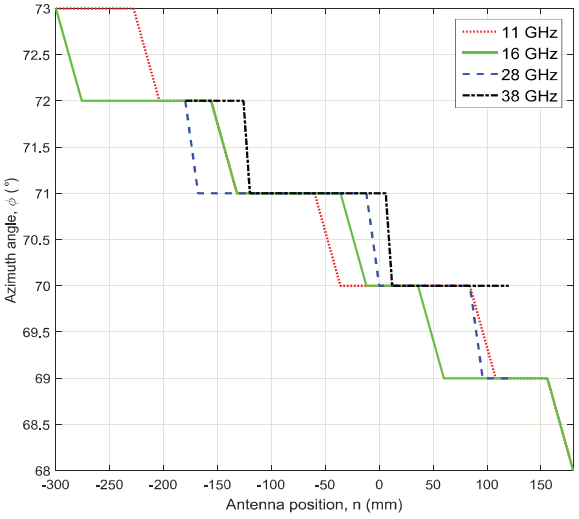


(d) Azimuth angle variations at Tx4

Fig. 2. (a) Azimuth angle variations at Tx1; (b) Azimuth angle variations at Tx2; (c) Azimuth angle variations at Tx3; (d) Azimuth angle variations at Tx4.

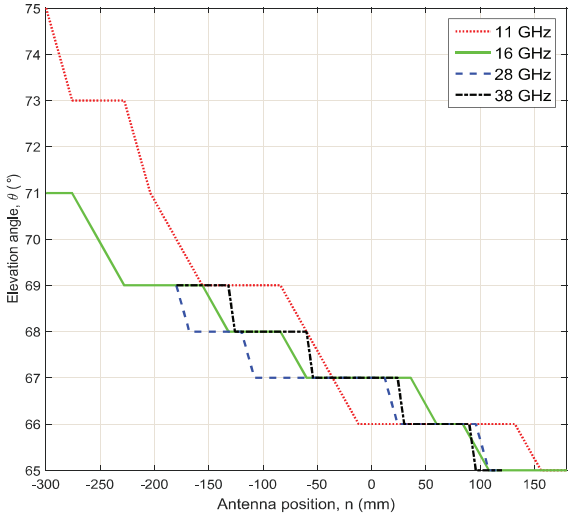


Fig. 3. Elevation angle variations at Tx4.

over the large array. The variations of the temporal-spatial parameters including delay, azimuth angle, and elevation angle can also be seen in Figs. 4–6. Fig. 8, Fig. 9, and Fig. 10 show the DS, azimuth AS, and elevation AS variations over the array at Tx4 location for the four bands, respectively. As shown in Fig. 8, the DS can vary in the range of 3 ns over the array. Fig. 9 shows that the azimuth AS can vary 20° over the array. Fig. 10 shows that the elevation AS variation is in the range of about 5° over the array. All the results indicate that the mmWave massive MIMO channel shows the non-stationarity property over the array and should not be seen as a WSS channel.

## V. Conclusions

In this paper, we have carried out massive MIMO channel measurements at 11, 16, 28, and 38 GHz frequency bands in an indoor office environment. The large antenna array has been divided into several sub-arrays. A sliding window has been used over the large array, and the SAGE algorithm has been applied to process the sub-array measurement data. New propagation characteristics caused by the large antenna array have been validated for 10–40 GHz mmWave bands. Especially,

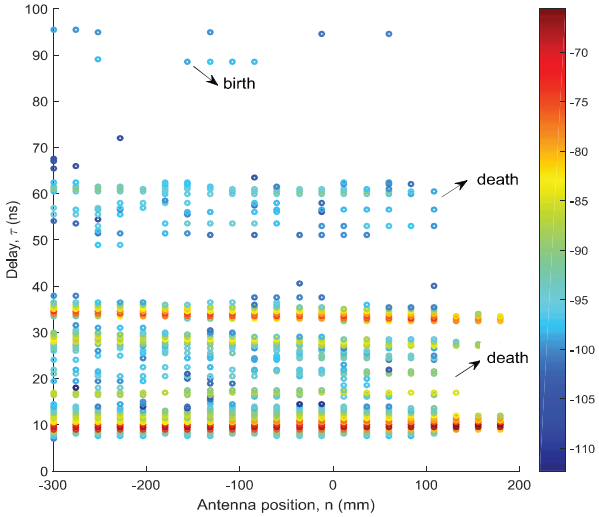


Fig. 4. PDP variations over the array for 16 GHz at Tx1.

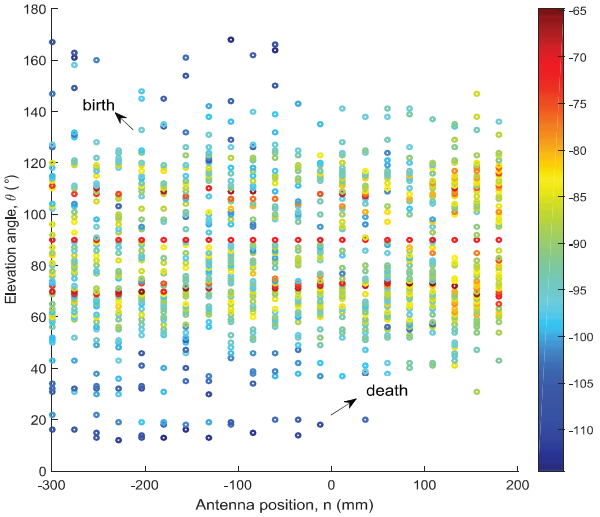


Fig. 6. PEP variations over the array for 16 GHz at Tx1.

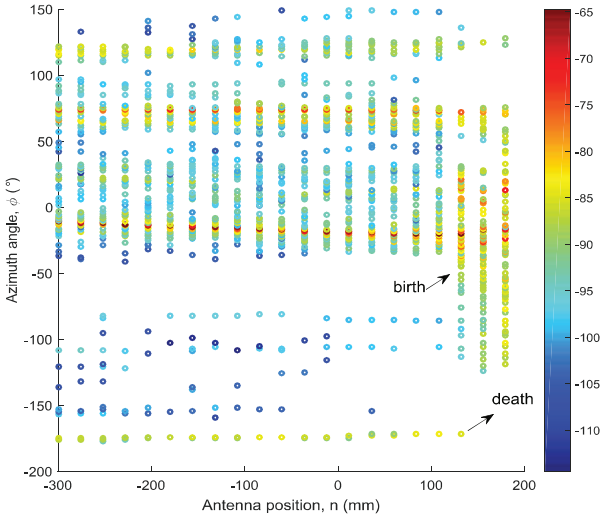


Fig. 5. PAP variations over the array for 16 GHz at Tx1.

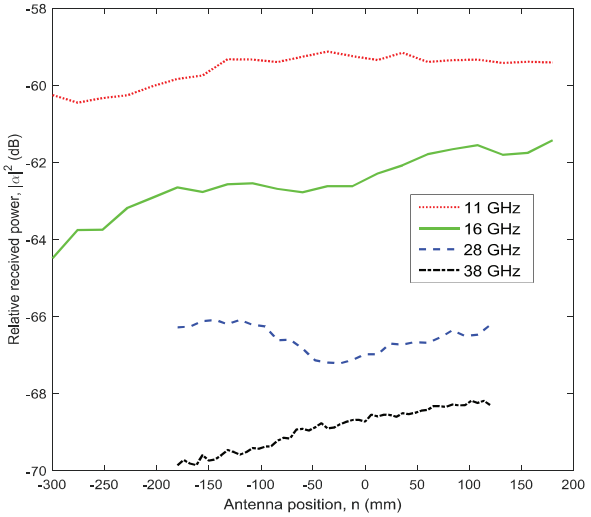


Fig. 7. LOS received power variations at Tx2.

the spherical wavefront property, cluster birth-death property, and non-stationarity over the array have been verified by investigating the temporal-spatial MPC parameter variations over the array, including the PDP, PAP, and PEP. The statistical property variations like RMS DS, azimuth AS, and elevation AS have also been characterized. The measurements, data processing, and analysis can easily be extended to other scenarios. These mmWave massive MIMO channel measurements and analysis have indicated that massive MIMO propagation characteristics should be considered for mmWave channel models under large antenna array systems.

## ACKNOWLEDGMENT

The authors would like to acknowledge the support from the EU H2020 ITN 5G Wireless project (Grant No. 641985), EU FP7 QUICK project (Grant No. PIRSES-GA-2013-612652), EPSRC TOUCAN project (Grant No. EP/L020009/1), National Science and Technology Major Project (Grant No. 2014ZX03003012-001), 863 Project in 5G (Grant No. 2014AA01A707), National Natural Science Foundation of China (Grant No. 61210002, 61371110), and the Science and Technology Commission of Shanghai Municipality (STCSM) under grant 14ZR1439700.

## REFERENCES

[1] C.-X. Wang, F. Haider, X. Gao, X.-H. You, Y. Yang, D. Yuan, H. Aggoune, H. Haas, S. Fletcher, and E. Hepsaydir, "Cellular architecture and key technologies for 5G wireless communication networks," *IEEE Commun. Mag.*, vol. 52, no. 2, pp. 122–130, Feb. 2014.

[2] T. S. Rappaport, G. R. MacCartney, M. K. Samimi, and S. Sun, "Wideband millimeter wave propagation measurements and channel models for future wireless communication system design," *IEEE Trans. Commun.*, vol. 63, no. 9, pp. 3029–3056, Sept. 2015.

[3] X. Gao, O. Edfors, F. Rusek, and F. Tufvesson, "Massive MIMO performance evaluation based on measured propagation data," *IEEE Trans. Wireless Commun.*, vol. 14, no. 7, pp. 3899–3911, Jul. 2015.

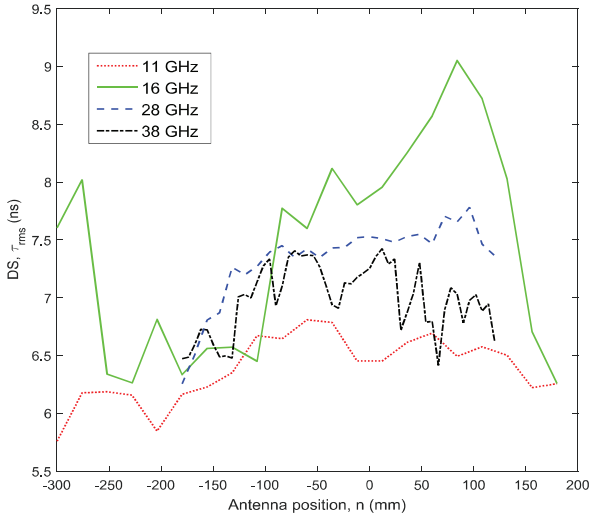


Fig. 8. DS variations at Tx4.

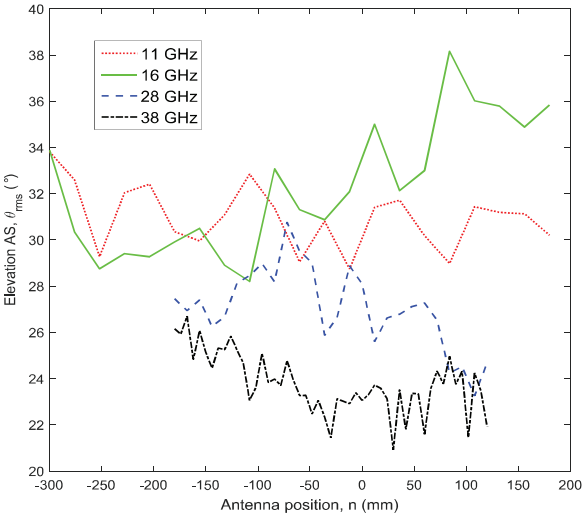


Fig. 10. Elevation AS variations at Tx4.

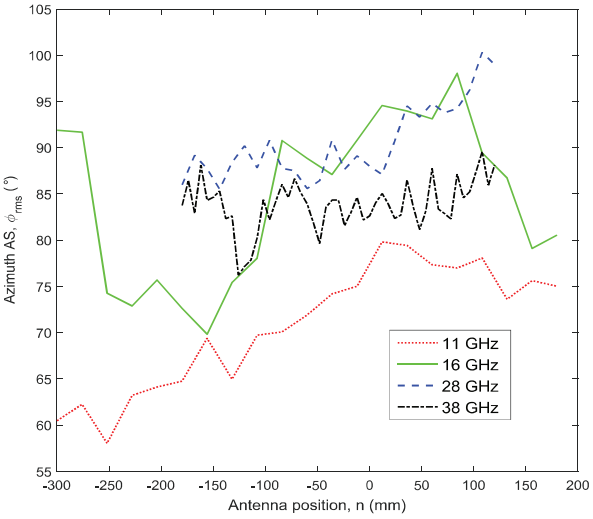


Fig. 9. Azimuth AS variations at Tx4.


[4] A. L. Swindlehurst, E. Ayanoglu, P. Heydari, and F. Capolino, "Millimeter-wave massive MIMO: The next wireless revolution?" *IEEE Commun. Mag.*, vol. 52, no. 9, pp. 3917–3928, Nov. 2015.

[5] C.-X. Wang, S. Wu, L. Bai, X. You, J. Wang, and C.-L. I, "Recent advances and future challenges for massive MIMO channel measurements and models," *Sci. China Inf. Sci.*, vol. 59, no. 2, pp. 1–16, Feb. 2016.

[6] S. Payami and F. Tufvesson, "Channel measurements and analysis for very large array systems at 2.6 GHz," in *Proc. EuCAP'12*, Prague, Czech, Mar. 2012, pp. 433–437.

[7] X. Gao, F. Tufvesson, O. Edfors, and F. Rusek, "Measured propagation characteristics for very-large MIMO at 2.6 GHz," in *Proc. ACSSC'12*, Pacific Grove, CA, USA, Nov. 2012, pp. 295–299.

[8] D. Fei, R. He, B. Ai, B. Zhang, K. Guan, Z. Zhong, "Massive MIMO channel measurements and analysis at 3.33 GHz," in *Proc. ChinaCom'15*, Shanghai, China, Aug. 2015, pp. 194–198.

[9] J. Li, B. Ai, R. He, K. Guan, Q. Wang, D. Fei, Z. Zhong, Z. Zhao, D. Miao, and H. Guan, "Measurement-based characterizations of indoor massive MIMO channels at 2 GHz, 4 GHz, and 6 GHz frequency bands," in *Proc. IEEE VTC'16-Spring*, Nanjing, China, May 2016, pp. 1–5.

[10] A. Taira, H. Iura, K. Nakagawa, S. Uchida, K. Ishioka, A. Okazaki, S. Suyama, T. Obara, Y. Okumura, and A. Okamura, "Performance evaluation of 44 GHz band massive MIMO based on channel measurement," in *Proc. IEEE Globecom'15*, San Diego, CA, USA, Dec. 2015, pp. 1–6.

[11] J. Chen, X. Yin, and S. Wang, "Measurement-based massive MIMO channel modeling in 13–17 GHz for indoor hall scenarios," in *Proc. IEEE ICC'16*, Kuala Lumpur, Malaysia, May 2016, pp. 1–5.

[12] X. Wu, C.-X. Wang, J. Sun, J. Huang, R. Feng, Y. Yang, and X. Ge, "60 GHz millimeter-wave channel measurements and modeling for indoor office environments," *IEEE Trans. Antennas Propag.*, 2017, in press.

[13] B. H. Fleury, M. Tschudin, R. Heddergott, D. Dahlhaus, and K. I. Pedersen, "Channel parameter estimation in mobile radio environments using the SAGE algorithm," *IEEE J. Sel. Areas Commun.*, vol. 17, no. 3, pp. 434–450, Mar. 1999.